Journal of Fluids and Structures 76 (2018) 527–535

Contents lists available at ScienceDirect

Journal of Fluids and Structures

journal homepage: www.elsevier.com/locate/jfs

Coupled motion of two side-by-side inverted flags

Cecilia Huertas-Cerdeira *, Boyu Fan [1], Morteza Gharib

Division of Engineering and Applied Science, California Institute of Technology, Pasadena, CA 91125, USA

HIGHLIGHTS

- Two side-by-side inverted flags can couple in the flapping regime.
- Five modes are present: in-phase, anti-phase, staggered, alternating and uncorrelated.
- An increase in amplitude and frequency of flapping was observed.
- Flags of different lengths couple for small length differences.

ARTICLE INFO

Article history:
Received 20 June 2017
Received in revised form 6 October 2017
Accepted 14 November 2017
Available online 1 December 2017

Keywords:
Inverted flag
Coupled dynamics
Synchronization

ABSTRACT

The interaction and coupling between two inverted flags that are placed side-by-side in a uniform flow is investigated in an effort to determine the behavior of systems that are formed by arrays of cantilevered plates. Inverted flags are elastic plates that are free to move at their leading edge and clamped at their trailing edge. We show that placing two inverted flags of equal dimensions side-by-side will cause their motion to couple. In-phase, anti-phase, staggered, alternating and decoupled flapping modes are present, with the anti-phase mode being predominant at small flag distances and low wind speeds. Increases both in amplitude and frequency of flapping are observed in the two flag system with respect to a single flag. Two side-by-side inverted flags of different lengths are found to interact for small length differences, with the longer flag being able to induce a motion on the shorter flag even when the latter is outside of its flapping wind speed range.

1. Introduction

The response of a flexible plate to an impinging flow has been the subject of a wide array of studies. From flexible leaflets in heart valves (Peskin, 1972) to flutter in paper processing (Watanabe et al., 2002) the interaction between thin sheet-like structures and a fluid is pervasive both in nature and engineering. These structures can present many different configurations depending on the boundary conditions of the plate, resulting in a large variety of behaviors. In particular, the flag configuration, where a thin elastic sheet is clamped to a pole and oriented in the direction of the flow, leaving a free trailing edge, has received recent attention (Shelley and Zhang, 2011). A number of engineering applications have arisen for the flag configuration, such as the use of its flapping motion to harvest energy from the wind (Taylor et al., 2001; Tang et al., 2009).

In nature, however, it is more often the case that flags present multiple orientations to the flow. Examples are the leaves of a tree, that are commonly found at varying angles to incoming wind. Considering this, Kim et al. (2013) studied an inverted flag configuration, where an elastic plate is free to move at its leading edge and clamped at its trailing edge. They found

* Corresponding author.
E-mail address: chuertas@caltech.edu (C. Huertas-Cerdeira).
[1] Present affiliation: Department of Mechanical Engineering, Massachusetts Institute of Technology, Cambridge, MA, 02139, USA.

https://doi.org/10.1016/j.jfluidstructs.2017.11.005
0889-9746/

the existence of three main dynamic regimes as the free stream velocity is increased: a small amplitude oscillation around the zero deflection position (straight regime), a large amplitude flapping motion (flapping regime) and a small amplitude oscillation around a deflected position (deflected regime). In the flapping regime the inverted flag experiences strains much larger than those of the conventional flag, making it particularly useful for energy harvesting (Gurugubelli and Jaiman, 2015). Kim et al. (2013) suggested, based on experimental observations, that this flapping motion is a vortex induced vibration. This conclusion has been numerically and theoretically verified by Gurugubelli and Jaiman (2015) and Sader et al. (2016a), respectively.

Our knowledge of vortex induced vibrations has advanced enormously in the past decades (for a review, see Williamson and Govardhan (2004)), with much of the literature being centered in the study of the vortex induced vibrations of cylinders. Interesting wake dynamics arise when two fixed stationary cylinders are immersed side-by-side in a flow (Zdravkovich (2003) and references therein). Depending on the separation between them, they have been shown to generate either a single vortex street, two wakes of different widths that present a bi-stable gap flow, two equal and synchronized wakes or two completely uncoupled wakes. In the case of cylinders that are flexible or allowed to move the coupling of the wakes can result in the coupling of the motion of the cylinders (Zdravkovich, 1985; Zhou et al., 2001; Liu et al., 2001; Huera-Huarte and Gharib, 2011).

Similarly, two conventional flags placed side-by-side in a flow have been shown to interact. Zhang et al. (2000) experimentally studied the motion of two side-by-side filaments immersed in a soap film and observed both an in-phase flapping mode for small flag separations and an anti-phase flapping mode for larger flag distances. The anti-phase mode was observed to oscillate with frequencies 35% higher than those of the in-phase mode. As the distance was further increased, the interaction weakened and the flags moved independently. Analogous results were obtained in numerical simulations by Zhu and Peskin (2003) and Farnell et al. (2004). Farnell et al. (2004), Si-Ying et al. (2013), Sun et al. (2016) observed, in addition to the in-phase and out of phase modes, the existence of a transition mode where the frequencies of both motions co-exist. A different transition mode was reported by Jia et al. (2007), who observed a region where in-phase and out-of phase flapping alternate randomly. In addition to two equal filaments, Jia et al. (2007) studied the motion of two side-by-side filaments whose length varied by a factor of two and observed synchronization with a scattering of the phase around the 0 and π values.

These interactions with neighboring flags and their vortex streets can cause variations in the forces experienced by the flags. Many natural organisms exploit the vortex street of neighboring bodies to enhance their performance; an example are schooling fish (Weihs, 1973). Inspired by this behavior, optimal arrangements of vertical axis wind turbines have been shown to increase energy extraction in wind farms (Whittlesey et al., 2010). Dong et al. (2016) showed that placing two flags side-by-side can produce increased energy extraction efficiency in a potential energy harvesting mechanism. It is expected that inverted flags will show a similar behavior, and placing several flags in close proximity may enhance their energy harvesting capabilities. Changes in phase between the swimming motion of adjacent fish can drastically change the effect of schooling (Weihs, 1973). This implies that in systems such as flags, where the phase between flags is determined by their relative position, the presence and arrangement of surrounding flags plays a double role and is particularly significant.

The purpose of this study is to experimentally investigate the coupling of the motion of two inverted flags when placed in a side-by-side arrangement. Because the amplitudes of oscillation of the inverted flag vary greatly between the different regimes of motion (straight, flapping and deflected), the effective cross-sectional area of the flag undergoes significant changes between them. This causes the synchronization in the motion of the flags to occur at very different flag separations for the different regimes. In this study we have focused on distances at which the flags never collide ($1.7 < T/L < 5.4$ with T the distance between flags and L the flag length), which are pertinent to the coupling of the vortex induced vibrations of the flags in the flapping and deflected regimes.

2. Experimental setup

The experiments were conducted in an open loop wind tunnel of test section 1.2 m $\times$ 1.2 m. A square array of 10 $\times$ 10 small fans generates uniform wind speeds between 2.2 m/s and 8.5 m/s. The turbulence intensity, measured using a hot wire probe, is under 8.2% for the range of wind speeds studied. The variation in wind speed across the cross section, caused by the multiplicity of fans, is smaller than 2.7%. A schematic of the setup is shown in Fig. 1a. The flags are made of polycarbonate (Young's modulus $E = 2.41$ GPa, Poisson ratio $\nu = 0.38$ and density $\rho_s = 1200$ kg m^{-3}) and have a thickness of $h = 0.254$ mm. They present initial edge deflections smaller than 5° due to the curvature induced by material defects. The flags will be labeled left flag and right flag throughout this article, corresponding to their position when the observer is located downstream of the flags. The first series of experiments was conducted with two flags of equal height $H = 150$ mm and length $L = 100$ mm. In the second series, the height of both flags, $H = 150$ mm, and the length of one of the flags, $L_0 = 100$ mm, were maintained constant, while the length of the second flag, L, was varied. The flags are clamped at their trailing edge by means of two aluminum bars of rectangular cross section of width 6 mm. They are clamped parallel to the flow, within 1° of the zero angle of attack. This error in the clamping angle, together with the initial curvature of the flag, introduce small variations in the motion of the flag (Cossé et al., 2014) and account for the majority of the variability in frequency and amplitude of flapping between the two equal flags. The bars are attached to a rail such that the distance between flags, T, can be varied and are placed vertically such that the deformation of the sheet is primarily in the horizontal plane, with no twisting due to gravity being observed. The motion of the flags is recorded from above at 100 frames per

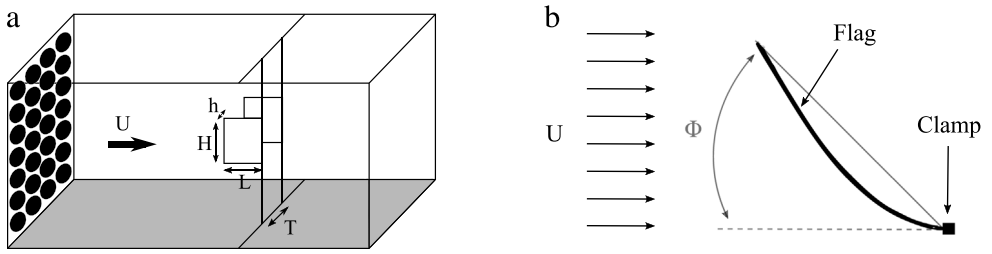

Fig. 1. (a) Schematic of the experimental setup, with notation for flag dimensions (b) Top view of a deflected inverted flag. The parameter ϕ used throughout this article is the angle between the free-stream velocity vector and the line joining the free end of the plate and the clamp.

second using a high speed camera (Imperx IPX-VGA210-L). The position of the flag at each frame is extracted using a Matlab script.

The motion of the flag is defined by means of the angle, ϕ, between the free-stream velocity vector and the line joining the leading edge and clamping point of the flag (see Fig. 1b). This parameter is used because it is monotonic in each half-cycle of flapping, with the vortices being shed at the maximum and minimum values. This differs from the amplitude used by previous studies (Kim et al., 2013), where a single value can correspond to two different positions even for a fixed wind speed and flag separation when the flag motion surpasses the 90° angle. The minimum edge to clamp distance is 60 pixels and the tracking script is observed to detect the flag edge within 4 pixels, resulting in errors in the measurement of ϕ smaller than 4°.

There are five non-dimensional parameters that are relevant in the motion of the side-by-side inverted flag system: dimensionless velocity, $\sqrt{\kappa}$, mass ratio, μ, aspect ratio, AR, dimensionless flag separation, $\widetilde{T}$ and Reynolds number Re. They are defined in the following way,

$$\kappa = \frac{\rho_f U^2 L^3}{D}, \qquad \mu = \frac{\rho_s h}{\rho_f L}, \qquad AR = \frac{H}{L}, \qquad \widetilde{T} = \frac{T}{L} \qquad Re = \frac{\rho U L}{\mu}$$

where $D = Eh^3/(12(1-\nu^2))$ is the stiffness of the flag, U is the free stream velocity, ρ_f is the density of the fluid and μ is the dynamic viscosity of the fluid. In this study the values of κ ranged between 0.63 and 34.3, those of μ between 2.36 and 3.1, those of the AR between 1.30 and 1.76, those of $\widetilde{T}$ between 1.7 and 5.4, and those of Re between 9.76×10^3 and 6.17×10^4. The characteristic features of the flag dynamics and vortex wake have been shown to be fairly insensitive to the Reynolds number for high values of Re such as those used in these experiments (Ryu et al., 2015; Tang et al., 2015; Shoele and Mittal, 2016), as well as to the mass ratio (Kim et al., 2013; Gurugubelli and Jaiman, 2015; Tang et al., 2015; Shoele and Mittal, 2016). For this reason, the effect of these parameters on the side-by-side flag arrangement has not been analyzed in this study. The value of the aspect ratio is large enough for the effect of vortex lift to be secondary to that of linear lift on the undeflected flag (Sader et al., 2016b).

3. Results and discussion

3.1. Flags of equal dimensions

The three main dynamic regimes present in the motion of a single flag (straight, flapping and deflected) as well as the chaotic motion described by Sader et al. (2016a) persist in the two flag system. For the distances $\widetilde{T}$ considered in this study and at low flow speeds (straight regime, Fig. 2a), the flags oscillate with small amplitude relative to the flag separation and no coupling occurs. As the wind speed is increased, the flag motion reaches angular amplitudes greater than 10°, giving rise to periodic vortex shedding and flapping (Sader et al., 2016a). The lower critical wind speed, κ_c, at which the flapping motion is onset was not observed to vary with the presence of the second flag. This is consistent with the onset of flapping occurring through an initial divergence instability that is dependent on the aerodynamic lift coefficient at small angles (Sader et al., 2016a). It is to be expected, however, that variations in the critical wind speed as well as synchronization in the straight regime will occur at flag separations smaller than those considered in this study.

In the flapping regime (Fig. 2b) the flags interact strongly. An increase in the angular amplitude of flapping of up to 36% was observed for the two flag system with respect to the single flag. Fig. 3 shows the peak-to-peak amplitude of motion, averaged between the right and left flags, for varying separation distances. As the distance between flags is increased the gain in amplitude becomes less prominent, saturating at the single flag value for $\widetilde{T} > 3.2$. This increase in amplitude is asymmetrical; as is evident from the stroboscopic progressions in Fig. 2b, the flags swipe a larger angle towards the interior (center) of the system. Small increases in frequency, up to 13%, were also observed at the smallest separations for the initial stages of the flapping regime. Increases both in the amplitude and frequency of flapping suggest that the energy available for harvesting in the two flag system is higher than that of the single flag.

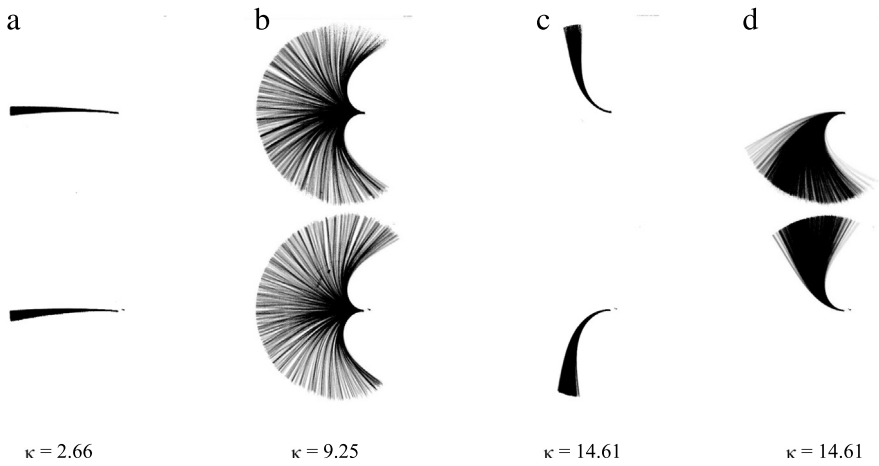

Fig. 2. Stroboscopic progressions of the motion of the two flag system showing the (a) straight regime, (b) flapping regime, (c) deflected regime in the outside-deflected configuration and (d) deflected regime in the inside-deflected configuration.

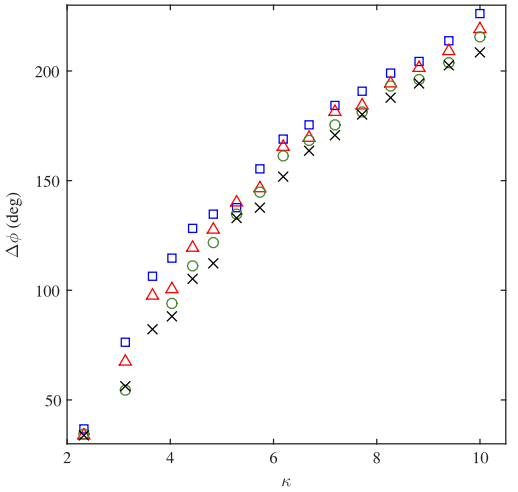

Fig. 3. Peak-to-peak angular amplitude of motion, $\Delta\phi$, in the flapping regime for a single flag ($\times$) and two flags separated by $\widetilde{T} = 2(\square)$, $\widetilde{T} = 2.4(\triangle)$ and $\widetilde{T} = 2.8(\circ)$. Represented values are the average of left and right flags.

Five different modes of flapping are present in the side-by-side inverted flag system. The angle ϕ of both flags as a function of time and the corresponding phase diagrams have been plotted in Fig. 4 for each of the modes. The phase diagrams have been colored to represent time: initially the curve is red and turns into blue as time advances. The modes include both an anti-phase regime (Fig. 4a), where the flags flap symmetrically, and an in-phase regime (Fig. 4b), where the flags flap anti-symmetrically. Staggered flapping, where the phase between flags is constant and between 0 and π, can also occur (Fig. 4c). In the alternating mode (Fig. 4d) the flags switch intermittently between two or more of the in-phase, anti-phase and staggered motions. This mode differs from the decoupled mode (Fig. 4e), where no coupling occurs, in the fact that the flags spend significantly more time in-phase, anti-phase and staggered than they do transitioning between the motions.

Because two identical flags have equal flapping frequency, they may appear to be flapping in-phase, anti-phase or staggered even if they are not interacting with each other. Therefore, in-phase, anti-phase or staggered modes have only been considered here when they constitute a steady state after starting from a different initial condition (see, for example, the phase diagram of staggered mode in Fig. 4c). In the current experiments, small variations in initial curvature, dimensions and angle of attack caused the frequencies of the right and left flags to differ, and therefore the phase between flags was observed to constantly change in the decoupled mode (Fig. 4e).

The relationship between wind speed, flag separation and flapping mode is summarized in Fig. 5. For small separations ($\widetilde{T} < 3.5$), the flags were observed to flap mainly in the anti-phase mode. For the same range of velocities an in-phase motion can also occur. However, the anti-phase mode is energetically favorable and any staggered initial conditions or perturbations in the in-phase mode will lead to anti-phase flapping. As the distance between flags is increased, the range of

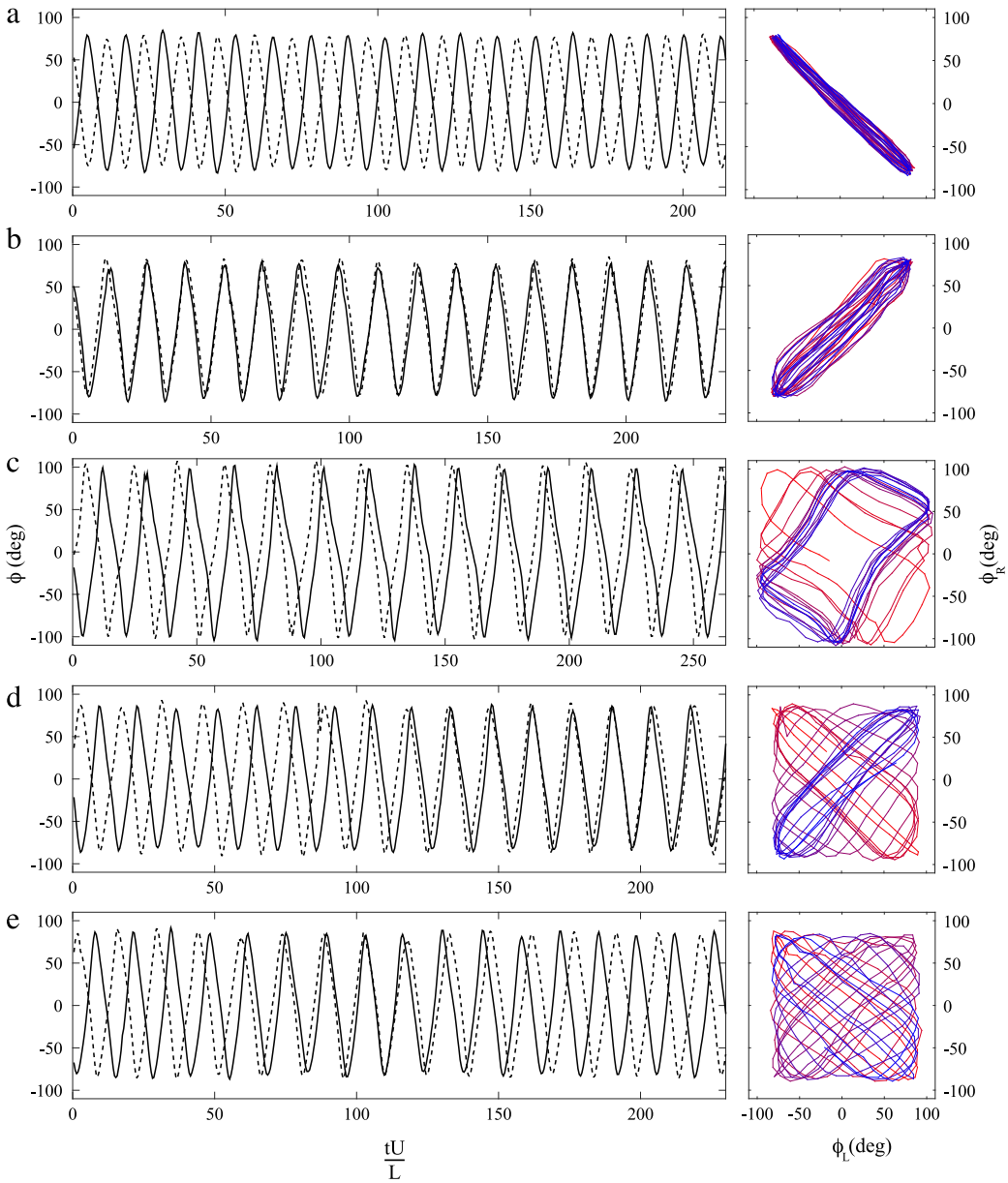

Fig. 4. Time history of the angle ϕ for the left flag (solid line) and right flag (dashed line) on the left and phase diagram on the right for (a) anti-phase, (b) in-phase, (c) staggered (d) alternating and (e) decoupled modes. Phase diagrams have been colored to represent time, with the curve being initially red and shifting to blue as time advances. (For interpretation of the references to color in this figure legend, the reader is referred to the web version of this article.)

velocities for which this predominantly anti-phase flapping is present decreases, giving rise to the staggered, in-phase and alternating modes. These appear for the higher wind speeds in the flapping range, whilst the anti-phase mode remains for the lower velocities. The distribution of staggered, in-phase and alternating modes for the different wind speeds and separation distances is not clearly defined. This suggests that as the anti-phase flapping becomes less energetically favorable several modes are possible, with different initial conditions giving rise to different modes and perturbations causing the flags to switch from one mode to the other. At a distance of $\widetilde{T} = 5$, the predominantly anti-phase flapping fully disappears. Finally, for large separation distances and high wind speeds the flags enter the decoupled regime, flapping uncoupled.

As wind speed is increased, the chaotic regime emerges. No synchronization was observed between the flags in this regime (see Fig. 6a). For wind speeds over a critical value the flags enter the deflected regime. No clear variations in the critical transition speed from the flapping to the deflected regimes have been observed for the two flag system with respect to a single flag. For flow speeds immediately over the transition speed the flags deflect towards the outside region, independently of the initial condition (as depicted in Fig. 2c). The oscillating motion of the flags around this outside deflected position is

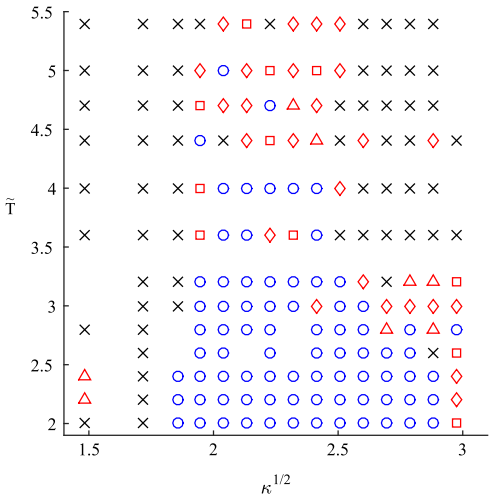

Fig. 5. Flapping modes as a function of the dimensionless wind speed, $\sqrt{\kappa}$ and flag separation, $\widetilde{T}$: (×) decoupled, (○) anti-phase, (△) in-phase, (□) staggered and (◇) alternating. Not all possible modes are represented in this figure.

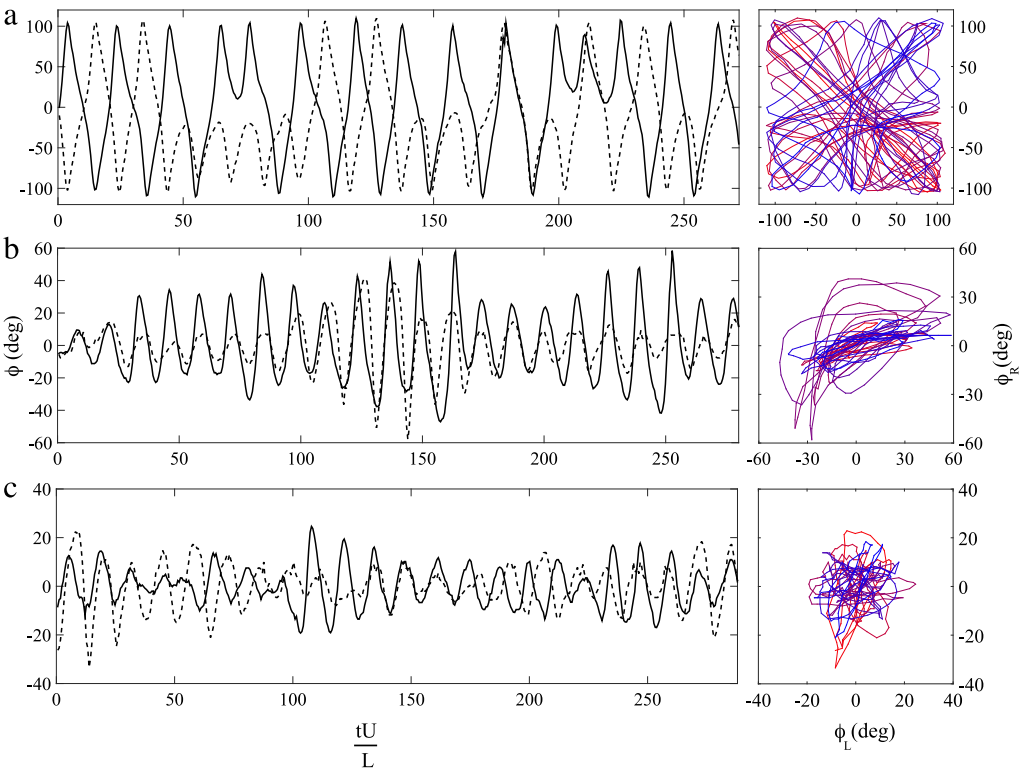

Fig. 6. Time history of the angle ϕ for the left flag (solid line) and right flag (dashed line) on the left and phase diagram on the right for (a) chaotic, (b) inside-deflected in-phase and (c) inside-deflected decoupled. Phase diagrams have been colored to represent time, with the curve being initially red and shifting to blue as time advances. For the deflected states (b) and (c) the average has been subtracted. (For interpretation of the references to color in this figure legend, the reader is referred to the web version of this article.)

independent, and therefore the flags only interact with each other at the initial stages, when they repel and force the outside deflected position. As flow speed is increased, however, the high fluid damping prevents the flags from changing side and inside (Fig. 2d), outside and asymmetric (one flag inside and one outside) deflected states are possible depending on the initial conditions. There is, again, no coupling between outside or asymmetrically deflected flags. However, inside-deflected flags can synchronize in-phase when considering oscillations around the deflected equilibrium (Fig. 6b). As speed is further increased synchronization ceases (Fig. 6c).

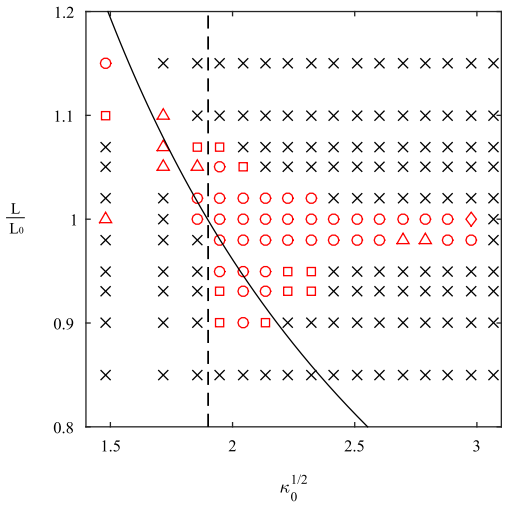

Fig. 7. Flapping modes as a function of the dimensionless wind speed, $\sqrt{\kappa_0}$ and the flag length ratio, (L/L_0): (×) decoupled, (○) anti-phase, (△) in-phase, (□) staggered and (◇) alternating. The distance between flags is constant ($T/L_0 = 2.4$). Lines represent the critical value of $\sqrt{\kappa_0}$ at which a single flag of length L_0 (dashed) and L (solid) enter the flapping regime.

3.2. Flags with different lengths

Flags that are equal in size have the same vortex shedding frequency, allowing for synchronization of the vortex streets and therefore of the motion of the flags. For flags of different lengths, on the other hand, the vortex shedding frequencies will not be equal. If these frequencies are sufficiently close, the vortex streets can still lock and synchronization will occur. Synchronization will cease, however, for flags that have significantly different lengths and therefore vortex shedding and natural frequencies. To study the effect of the relative length of the flags, a number of tests were performed in which the left flag was kept at a constant length, $L_0 = 0.1$ m, while the length of the right flag, L, was varied. The distance between flags was maintained constant at $T/L_0 = 2.4$. The results are plotted in Fig. 7, where the length used for the dimensionless variable κ_0 is that of the left constant flag ($L_0 = 0.1$ m).

For flags of the same length the results are equal to those reported in Section 3.1. The flags synchronize anti-phase for most of the velocities in the flapping range, although staggered modes are also present. As L is decreased, the range of velocities at which the flags synchronize decreases; at $\frac{L}{L_0} \leq 0.85$ synchronization ceases to occur. Simultaneously, the anti-phase mode becomes less predominant, with the staggered mode being more prevalent. Similarly, as L is increased from the $\frac{L}{L_0} = 1$ value, the range of wind speeds at which the flags synchronize decreases and the anti-phase mode vanishes in favor of in-phase and staggered motions.

Because the variations in aspect ratio are small, the critical value of κ at which both flags enter the flapping regime is approximately equal. Due to the difference in length, however, this corresponds to different values of the dimensional wind speed, meaning that there is a range of wind speeds at which the longer flag is in the flapping regime whilst the shorter one is in the straight regime. To identify these regions, the lines corresponding to the critical dimensionless velocity $\kappa_0 = \kappa_c$ for each of the flags, as given by equation (2.15) in Sader et al. (2016b), have been plotted in Fig. 7. The dashed line corresponds to the critical κ for the flag of constant length L_0, while the solid line corresponds to that of the flag of varying length L. The equation slightly overestimates the value of κ_c that was experimentally observed, including the case of a single flag, presumably due to small variations in flow uniformity and initial curvature.

For $\frac{L}{L_0} < 1$, the flag of length L_0 reaches its flapping range at lower flow speeds than the flag of length L. As is evident in Fig. 7, despite the fact that the flag of length L is under its critical κ, synchronization, mostly in an anti-phase mode, still occurs. The flag of length L was observed to flap in these conditions (Fig. 8a), implying that the motion and resulting vortex street of the longer flag is inducing a flapping motion in the shorter flag. For the opposite case, $\frac{L}{L_0} > 1$, a similar behavior was observed: synchronization occurs for wind speeds at which the flag of length L has reached its flapping regime but that of length L_0 has not. In this case, however, the shorter flag does not flap, but oscillates with small amplitude (Fig. 8b). These oscillations are in phase with the flapping motion of the longer flag and are larger than the oscillations that occur when the flags move uncoupled (Fig. 8c). This leads to the conclusion that it is the flow displaced by the flapping flag that impinges on the short flag and causes it to deflect. These two different behaviors (induced flapping and induced oscillations) in a seemingly symmetric problem arise because the distance between flags was maintained at a constant value and, therefore, the relative distance T/L is different in the two cases, with the flags being effectively closer in the $\frac{L}{L_0} > 1$ case.

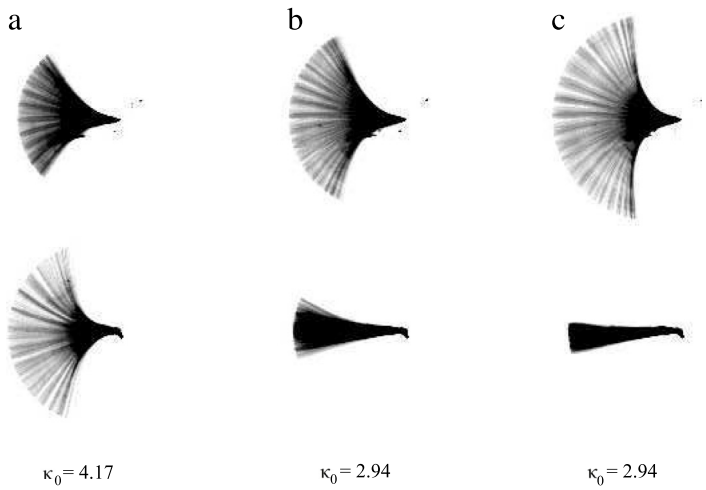

Fig. 8. Stroboscopic progressions of the motion of two inverted flags of different lengths at a constant separation $T/L_0 = 2.4$., showing (a) the long flag inducing a flapping motion on the short flag ($L/L_0 = 0.9$), (b) the long flag inducing an oscillating motion on the short flag ($L/L_0 = 1.05$) and (c) the long flag flapping and the short flag oscillating uncoupled ($L/L_0 = 1.15$). The flag of constant length $L_0 = 0.1$ m is depicted at the bottom.

4. Conclusions

This study has experimentally investigated the interaction between two inverted flags that are placed side-by-side in a uniform flow and the resulting coupled motion in the flapping and deflected regimes. It is relevant to the analysis of natural phenomena, such as leaves flapping in the wind, where multiple flags are generally present, as well as to the design of energy harvesting mechanisms, where the arrangement of multiple flags could be exploited to increase energy extraction.

Flags that were placed side-by-side saw an increase in flapping angular amplitude of up to 36% and an increase in frequency of up to 13% with respect to the motion of a single flag. Five different coupled modes of motion were observed in the flapping regime: in-phase, anti-phase, staggered, alternating and decoupled. The anti-phase mode is energetically favorable and predominant for small separations and low wind speeds, while the remaining modes appear for larger separations and high wind speeds. Inside, outside and asymmetric configurations are present in the deflected regime, with the inside configuration being the only one that presents a coupled in-phase motion.

Coupling was observed to occur between flags that had different lengths. However, the range of velocities at which coupling occurred was observed to diminish as the difference in flag lengths increased, with no coupling occurring for differences larger than 15%. Interestingly, the longer flag was observed to induce flapping on the shorter flag when the latter was outside of its flapping range.

Our work has addressed the kinematics of the side-by-side inverted-flag system, however, a more detailed analysis of its dynamics will aid to extend these results to potential applications. Compelling avenues for future work are the study of the coupling between flags that are placed at distances short enough such that collision is possible, as well as the study of the power extraction enhancement characteristics of the two-flag system.

Acknowledgments

This research was supported by the Gordon and Betty Moore Foundation and the Charyk Family Foundation. Cecilia Huertas-Cerdeira acknowledges support through the la Caixa Fellowship Grant for Post-Graduate Studies, la Caixa Banking Foundation, Barcelona, Spain. The authors acknowledge the aid of Antoine Barizien in conducting the experiments.

References

Cossé, J., Sader, J., Kim, D., Cerdeira, C.H., Gharib, M., 2014. The effect of aspect ratio and angle of attack on the transition regions of the inverted flag instability. In: Proc. ASME.

Dong, D., Chen, W., Shi, S., 2016. Coupling motion and energy harvesting of two side-by-side flexible plates in a 3D uniform flow. Appl. Sci. 6 (5), 141.

Farnell, D.J., David, T., Barton, D., 2004. Coupled states of flapping flags. J. Fluids Struct. 19 (1), 29–36.

Gurugubelli, P., Jaiman, R., 2015. Self-induced flapping dynamics of a flexible inverted foil in a uniform flow. J. Fluid Mech. 781, 657–694.

Huera-Huarte, F., Gharib, M., 2011. Flow-induced vibrations of a side-by-side arrangement of two flexible circular cylinders. J. Fluids Struct. 27 (3), 354–366.

Jia, L.-B., Li, F., Yin, X.-Z., Yin, X.-Y., 2007. Coupling modes between two flapping filaments. J. Fluid Mech. 581, 199–220.

Kim, D., Cossé, J., Cerdeira, C.H., Gharib, M., 2013. Flapping dynamics of an inverted flag. J. Fluid Mech. 736, R1.

Liu, Y., So, R., Lau, Y., Zhou, Y., 2001. Numerical studies of two side-by-side elastic cylinders in a cross-flow. J. Fluids Struct. 15 (7), 1009–1030.

Peskin, C.S., 1972. Flow patterns around heart valves: a numerical method. J. Comput. Phys. 10 (2), 252–271.

Ryu, J., Park, S.G., Kim, B., Sung, H.J., 2015. Flapping dynamics of an inverted flag in a uniform flow. J. Fluids Struct. 57, 159–169.
Sader, J.E., Cossé, J., Kim, D., Fan, B., Gharib, M., 2016a. Large-amplitude flapping of an inverted flag in a uniform steady flow–a vortex-induced vibration. J. Fluid Mech. 793, 524–555.
Sader, J.E., Huertas-Cerdeira, C., Gharib, M., 2016b. Stability of slender inverted flags and rods in uniform steady flow. J. Fluid Mech. 809, 873–894.
Shelley, M.J., Zhang, J., 2011. Flapping and bending bodies interacting with fluid flows. Annu. Rev. Fluid Mech. 43, 449–465.
Shoele, K., Mittal, R., 2016. Energy harvesting by flow-induced flutter in a simple model of an inverted piezoelectric flag. J. Fluid Mech. 790, 582–606.
Si-Ying, W., Wen-Gang, D., Xie-Zhen, Y., 2013. Transition mode of two parallel flags in uniform flow. Chin. Phys. Lett. 30 (11), 110502.
Sun, C., Wang, S., Jia, L., Yin, X., 2016. Force measurement on coupled flapping flags in uniform flow. J. Fluids Struct. 61, 339–346.
Tang, C., Liu, N.-S., Lu, X.-Y., 2015. Dynamics of an inverted flexible plate in a uniform flow. Phys. Fluids 27 (7), 073601.
Tang, L., Païdoussis, M.P., Jiang, J., 2009. Cantilevered flexible plates in axial flow: energy transfer and the concept of flutter-mill. J. Sound Vib. 326 (1), 263–276.
Taylor, G.W., Burns, J.R., Kammann, S.M., Powers, W.B., Wel, T.R., 2001. The energy harvesting eel: a small subsurface ocean/river power generator. IEEE J. Ocean. Eng. 26 (4), 539–547.
Watanabe, Y., Suzuki, S., Sugihara, M., Sueoka, Y., 2002. An experimental study of paper flutter. J. Fluids Struct. 16 (4), 529–542.
Weihs, D., 1973. Hydromechanics of fish schooling. Nature 241 (5387), 290–291.
Whittlesey, R.W., Liska, S., Dabiri, J.O., 2010. Fish schooling as a basis for vertical axis wind turbine farm design. Bioinspiration Biomimetics 5 (3), 035005.
Williamson, C., Govardhan, R., 2004. Vortex-induced vibrations. Annu. Rev. Fluid Mech. 36, 413–455.
Zdravkovich, M., 1985. Flow induced oscillations of two interfering circular cylinders. J. Sound Vib. 101 (4), 511–521.
Zdravkovich, M.M., 2003. Flow Around Circular Cylinders: Volume 2: Applications, Vol. 2. Oxford university press.
Zhang, J., Childress, S., Libchaber, A., Shelley, M., 2000. Flexible filaments in a flowing soap film as a model for one-dimensional flags in a two-dimensional wind. Nature 408 (6814), 835–839.
Zhou, Y., Wang, Z., So, R., Xu, S., Jin, W., 2001. Free vibrations of two side-by-side cylinders in a cross-flow. J. Fluid Mech. 443, 197–229.
Zhu, L., Peskin, C.S., 2003. Interaction of two flapping filaments in a flowing soap film. Phys. Fluids (1994-Present) 15 (7), 1954–1960.